Constructing Stochastic Models for Dipole Fluctuations from Paleomagnetic Observations

Bruce Buffett[a], Abhijit Puranam[b]

[a]*Department of Earth and Planetary Science, University of California, Berkeley, CA 94720, USA (bbuffett@berkeley.edu)*
[b]*Division of Geological & Planetary Sciences, Caltech, Pasadena, CA 91125, USA*

Abstract

Measurements of relative paleointensity are subject to temporal averaging and random error. Both of these errors limit our ability to construct stochastic models from paleomagnetic observations. Most of the difficulties for dipole fluctuations occur at high frequencies. We exploit this behavior to construct a stochastic model from two recent inversions of paleomagnetic observations for the axial dipole moment. An estimate of the noise term in the stochastic model is recovered from a high-resolution inversion (CALS10K2), while the drift term is estimated from the low-frequency part of the power spectrum for a long, but lower-resolution inversion (PADM2M). Realizations of the resulting stochastic model yield a composite, broadband power spectrum that agrees well with the spectra from both PADM2M and CALS10K2. A simple generalization of the stochastic model permits predictions for the mean rate of magnetic reversals. We show that the reversal rate depends on the time-averaged dipole moment, the variance of the dipole moment and a slow timescale that characterizes the adjustment of the dipole toward the time-averaged value. Predictions of the stochastic model give a mean rate of 4.2 Myr^{-1}, which is in good agreement with observations from marine magnetic

anomalies. We also show that the observed reversal rate is dependent on the temporal resolution of the observations.
Keywords: geodynamo, geomagnetic spectrum, stochastic model

1. Introduction

The spectrum of fluctuations in the geomagnetic dipole offer insights into the origin of the magnetic field and the dynamics of Earth's core (Constable and Johnson, 2005). Each distinct timescale bears the fingerprints of the underlying physical processes (e.g. Sakuraba and Hamano, 2007). Paleomagnetic observations are essential for characterizing the long-term behavior, yet no single source of information is sufficient to capture the full range of dynamics. Instead, an integrated approach is needed to combine different types of measurements into a composite record that spans a broad range of timescales.

One important source of information comes from measurements of relative paleointensity in marine sediments (Valet, 2003). Records are stacked and calibrated using independent estimates of absolute paleointensity to produce models for the virtual axial dipole moment (VADM) over the past two million years (Valet et al., 2005; Ziegler et al., 2011). Sediments acquire a magnetization over several thousand years (Roberts and Winkholfer, 2004), so the true signal is averaged in time. Uncertainties in dating can have a similar affect because paleomagnetic records from different times may be stacked together.

Higher resolution records have been obtained for the past 10 kyr using a combination of archeomagnetic and lake sediment data. These data have

improved spatial resolution, so the geomagnetic field can be expanded in low-degree spherical harmonics (e.g. Korte and Constable, 2011). Even higher resolution records are available from historical observations (Jackson et al., 2000). Taken together these records provide a comprehensive description of fluctuations in the dipole field, but the task of combining these results into a single coherent model is a challenge.

Stochastic models are a useful tool because they enable quantitative predictions over a range of timescales. This facility is important for combining different types of data with different levels of temporal resolution. There is also good reason to think that stochastic models can represent the relevant processes in the core. Stochastic models have been constructed from geodynamo simulations with only a few model parameters, yet these models are able to reproduce most of the variability in these simulations (Kuipers et al., 2009; Buffett et al., 2014; Bouligand et al., 2016).

Synthetic studies using geodynamo simulations are an ideal test of the general approach because the simulations have relatively low numerical error and we can control the temporal resolution of the output. None of these advantages are available when we apply stochastic models to paleomagnetic observations. Significant errors are present in the estimates of the dipole field, which affect the construction of the stochastic model. We also need to deal with temporal averaging because it limits our ability to sample the stochastic process. The goal of this study is to address the practical limitations of dealing with paleomagnetic observations and to devise a strategy for constructing models that best explain both paleomagnetic and historical records. We focus primarily on the power spectrum of dipole fluctuations,

47 although we find that the resulting stochastic models can also account for
48 the observed reversal rate and the duration of polarity transitions.

49 2. Stochastic Description of Dipole Fluctuations

50 Stochastic models were introduced by Langevin (1908) to describe Brow-
51 nian motion. A small particle in water was assumed to move under the
52 combined influence of viscous resistance and a random force due to collision
53 with (unseen) water molecules. The viscous force was treated as a slowly
54 varying deterministic quantity, whereas the force due to collisions with water
55 molecules was treated as a rapidly fluctuating random process.

56 Brownian motion serves as a loose analogy for the evolution of the ge-
57 omagnetic dipole moment. The deterministic part of the dipole moment
58 can be represented by the opposing influences of dipole decay and the time-
59 averaged dipole generation. Rapid fluctuations in dipole generation about
60 the time average can be attributed to (unseen) turbulent flow, which we
61 treat as a random process. We denote the axial dipole moment by $x(t)$
62 and describe its time evolution using a stochastic differential equation (Van
63 Kampen, 1992)

$$\frac{dx}{dt} = v(x) + \sqrt{D(x)}\Gamma(t)\,, \tag{1}$$

64 where the drift term, $v(x)$, describes the deterministic part of the evolution
65 and the noise term, $D(x)$, defines the amplitude of the random part. The
66 time dependence of the random process, $\Gamma(t)$, is assumed to be Gaussian
67 with a vanishing time average

$$< \Gamma(t) >= 0\,. \tag{2}$$

We also assume that the correlation time of the noise source is short compared with the sampling of $x(t)$. In this case the autocovariance function of $\Gamma(t)$ can be approximated by a Dirac delta function,

$$< \Gamma(t_1)\Gamma(t_2) >= 2\delta(t_1 - t_2)\,, \tag{3}$$

where the factor of two is a common convention (e.g. Risken, 1989).

Estimates for $v(x)$ and $D(x)$ can be extracted from a realization of the stochastic process (e.g. Friedrich et al., 2011). The drift term is defined by

$$< x(t + \Delta t) - x(t) >= v(x)\Delta t + O(\Delta t^2) \tag{4}$$

and the noise term can be approximated by

$$< [x(t + \Delta t) - x(t)]^2 >= 2D(x)\Delta t + O(\Delta t^2)\,, \tag{5}$$

where the time averages are taken for a specific value of $x = x(t)$. In practice, the dipole moment is divided into a finite number of bins and the time average is evaluated for each bin. The time increment, Δt, is chosen to be long enough that $\Gamma(t)$ and $\Gamma(t+\Delta t)$ are uncorrelated, but short enough that higher order terms in Δt are small enough to neglect.

Applying (4) and (5) to the output of a geodynamo model (Buffett et al., 2014; Meduri and Wicht, 2016) shows that the drift term, $v(x)$, is well represented by

$$v(x) = -\gamma(x - < x >)\,, \tag{6}$$

where $< x >$ denotes the time average and γ is a constant that defines the inverse timescale for slow adjustments of the dipole. A similar representation for $v(x)$ has been recovered from VADM estimates (Brendel et al., 2007;

Buffett et al., 2013). Indeed very similar values for the constant, $\gamma \approx 34$ Myr^{-1}, are reported for the SINT-2000 model of Valet et al. (2005) and the PADM2M model of Ziegler et al. (2011). By comparison, the noise term, $D(x)$, has a weaker dependence on x. It suffices for our purposes to adopt the approximation $D(x) = D_{eq}$, where D_{eq} denotes the value of the noise term at $x =< x >$.

Simple representations for the drift and noise terms permit closed-form solutions for the power spectrum of fluctuations about the time average (e.g. $\epsilon(t) = x(t) - < x >$). Defining the Fourier transform of $\epsilon(t)$ by

$$\epsilon(f) = \int_{-\infty}^{\infty} \epsilon(t) e^{-i2\pi ft}\, dt\,, \tag{7}$$

the power spectrum becomes (Buffett and Matsui, 2015)

$$S_\epsilon(f) = \epsilon(f)\epsilon(f)^* = \frac{D_{eq}}{(\gamma^2 + 4\pi^2 f^2)} S_\Gamma(f)\,, \tag{8}$$

where the power spectrum of the noise is

$$S_\Gamma(f) = \Gamma(f)\Gamma(f)^* = 2\,. \tag{9}$$

Here * denotes the complex conjugate.

The theoretical spectrum in (8) agrees well with a direct calculation of the power spectrum from a geodynamo model (see Fig. 1). Departures at high frequency can be improved by allowing for the influence of correlated noise (see Buffett and Matsui, 2015, for details). The resulting spectrum for correlated noise (denoted by $S_\epsilon^c(f)$) reduces the power at high frequencies, but it does not change the behavior at low frequencies. It is important to note that the drift and noise terms are recovered from the geodynamo model using (4) and (5) with a time difference of $\Delta t = 1$ kyr. No long-period information

goes into the estimation of $v(x)$ and $D(x)$, yet the resulting predictions are in good agreement with the low-frequency part of the spectrum. This result suggests that simple stochastic models offer a good description of long-period dipole fluctuations.

3. Recovering the Drift and Noise from Paleomagnetic Models

Several complications arise when the drift and noise terms are computed from paleomagnetic models of the dipole moment. One complication is due to random error and the other is due to temporal averaging of the fluctuations. We explore both of these complications before proposing a possible solution.

3.1. Influence of Random Error

Random error alters the estimates of the dipole moment, so the drift and noise terms are computed from

$$y(t) = x(t) + \eta(t) \tag{10}$$

which includes a time-dependent error $\eta(t)$. The drift term becomes

$$v(y) = \frac{< y(t + \Delta t) - y(t) >}{\Delta t} \tag{11}$$

or

$$v(y) = v(x) + \frac{< \eta(t + \Delta t) - \eta(t) >}{\Delta t} \tag{12}$$

on substituting for $y(t)$ from (10). The presence of random error alters $v(y)$ but the time average of the error in (12) is expected to vanish. The same is not true for the noise term. Using $y(t)$ to evaluate $D(y)$ gives

$$D(y) = \frac{< [y(t + \Delta t) - y(t)]^2 >}{2\Delta t} \tag{13}$$

which can be rearranged into the form

$$D(y) = D(x) + \frac{< \Delta x \Delta \eta >}{\Delta t} + \frac{< \Delta \eta^2 >}{2\Delta t} \tag{14}$$

on introducing $\Delta x = x(t + \Delta t) - x(t)$ and $\Delta \eta = \eta(t + \Delta t) - \eta(t)$. Even when Δx and $\Delta \eta$ are uncorrelated and $\eta(t)$ represents the effects of white noise, we are left with (Hoze and Holeman, 2015)

$$D(y) = D(x) + \frac{\sigma_\eta^2}{\Delta t} \tag{15}$$

where σ_η^2 is the variance of the error. Thus the influence of random error becomes acute when Δt is small. On the other hand, larger Δt causes the higher order terms in (4) and (5) to become more important.

We illustrate the problem using a synthetic example. Consider a stochastic model with a linear drift term ($\gamma = 34$ Myr^{-1} or 0.034 kyr^{-1}) and a constant noise term ($D_{eq} = 69 \times 10^{44}$ A^2 m^4 Myr^{-1} or 0.069×10^{44} A^2 m^4 kyr^{-1}). These numerical values were recovered by Buffett et al. (2013) from model PADM2M of Ziegler et al. (2011). A numerical realization of the stochastic model is run for 2 Myr with values of $x(t)$ recorded at 1 kyr intervals. Next we add uncorrelated and normally distributed random error to produce a noisy record, $y(t)$, where the standard deviation of the error is $\sigma_\eta = 0.5 \times 10^{22}$ A m^2. Finally, we recover $D(x)$ and $D(y)$ from $x(t)$ and $y(t)$, respectively, assuming that both terms are independent of the amplitude of the dipole moment (i.e. a single bin for both x or y).

Figure 2 shows the estimates for $D(x)$ and $D(y)$ as a function of Δt. At the shortest time difference, $\Delta t = 1$ kyr, we obtain $D(x) = 0.068 \pm 0.002 \times 10^{44}$ A^2 m^4 kyr^{-1} and $D(y) = 0.297 \pm 0.010 \times 10^{44}$ A^2 m^4 kyr^{-1}, where the uncertainties represent one standard deviation. These results are consistent

with expectations from (15). Large deviations from the true value of D are found with the noisy record when Δt is small. Smaller deviations occur as Δt increases, although these errors remain relatively large. On the other hand, the value recovered from the error-free record, $x(t)$, is reliable at small Δt but departs from the known value as Δt becomes larger. Consequently, we cannot deal with the influence of random error by arbitrarily increasing Δt.

3.2. Influence of Temporal Averaging

Temporal averaging of the paleomagnetic record can arise in several ways. Errors in dating allows measurements at different times to be stacked. In addition, magnetization is acquired in sediments over several thousand years (Roberts and Winkholfer, 2004). A prolonged acquisition time removes high-frequency variations and affects our ability to sample the stochastic process at short Δt. One way to deal with the problem of averaging is to treat the measured record as a filtered version of the true signal (e.g. Leonard, 1974). We define the measured signal, $\bar{x}(t)$, as

$$\bar{x}(t) = \int_{-\infty}^{\infty} x(t')g(t-t')\,dt \tag{16}$$

where the filter function, $g(t)$, smooths the true signal, $x(t)$, over some prescribed time interval (denoted by T). Two popular filter functions are the box-car and gaussian filters (see Fig. 3). The true signal is convolved with a suitable filter function to produce the measured record.

The paleomagnetic record, $\bar{x}(t)$, still obeys a stochastic differential equation, but it is not the same as the differential equation in (1). Applying the filter to (1) gives

$$\frac{d\bar{x}}{dt} = -\gamma(\bar{x} - < x >) + D_{eq}\bar{\Gamma}(t) \tag{17}$$

where we have adopted a constant noise term and a linear drift term. The only difference in (17) is that the random process is driven by $\bar{\Gamma}(t)$ rather than $\Gamma(t)$. A power spectrum for $\bar{\epsilon} = \bar{x} - < x >$ is defined by taking the Fourier transform of (17). Solving for $\bar{\epsilon}(f)$ gives

$$S_{\bar{\epsilon}}(f) = \bar{\epsilon}(f)\bar{\epsilon}(f)^* = \frac{D_{eq}}{(\gamma^2 + 4\pi^2 f^2)} S_{\bar{\Gamma}}(f) \tag{18}$$

where

$$S_{\bar{\Gamma}}(f) = \bar{\Gamma}(f)\bar{\Gamma}(f)^* = 2\, g(f)\, g(f)^* \tag{19}$$

and $g(f)$ is the Fourier transform of the filter function. Equation (19) follows from the convolution theorem (e.g. Bracewell, 1999) because convolution in the time domain

$$\bar{\Gamma}(t) = \int_{-\infty}^{\infty} \Gamma(t') g(t - t')\, dt \tag{20}$$

corresponds to multiplication in the frequency domain

$$\bar{\Gamma}(f) = \Gamma(f) g(f)\,. \tag{21}$$

Power spectra for $x(t)$ and $\bar{x}(t)$ are the same at low frequencies because $g(f) \to 1$ as $f \to 0$ (see Fig 3).

We illustrate the consequences of time averaging using the stochastic model from Section 3.1. A 2-Myr realization is sampled at 1-kyr intervals and a smoothed version is produced using a box-car filter with an averaging time of $T = 3$ kyr. Figure 4 shows the power spectrum of the filtered signal, $\bar{x}(t)$, compared with the theoretical spectrum from (18). We also show the power spectrum for the original (unfiltered) time series, $x(t)$, versus the theoretical spectrum from (8). Both theoretical spectra are in good agreement with the direct calculations from $x(t)$ and $\bar{x}(t)$. Undulations in the spectrum of $\bar{x}(t)$ is

a consequence of the box-car filter, which is oscillatory in the Fourier domain. The main conclusion from this example is that temporal averaging affects only the high-frequency behavior of the record. The filtered dipole moment still obeys a stochastic differential equation and the spectrum is still reliably predicted at low frequencies from the drift and noise terms. Conversely, the low-frequency part of the spectrum constrains the drift and noise terms of the stochastic model.

Figure 5 shows the noise term, D, recovered from $x(t)$ and $\bar{x}(t)$ as a function of Δt. The most reliable estimate for D comes from $x(t)$ at the shortest possible Δt (1 kyr in this case). Temporal filtering substantially reduces the estimate of D at low Δt, although the recovered value approaches a constant once Δt exceeds the filter width T. A rule of thumb based on the spectrum of the filter (say $g(f) > 0.9$) is that Δt should be roughly twice T. Sampling the process at $\Delta t = 6$ kyr gives an estimate for D that is nearly independent of Δt. Unfortunately, this estimate is well below the known value (e.g. 0.044 versus 0.069). A similar departure in D at $\Delta t = 6$ kyr is inferred from $x(t)$ (e.g. 0.063 versus 0.069), although the error from the unfiltered time series is much smaller.

The preceding results show that temporal averaging can affect the amplitude noise term, particularly when Δt is smaller than the duration of the averaging. Estimates for D appear to approach a constant value once $\Delta t > 2T$, although this constant can be significantly less than the true value. On the other hand, random noise causes the recovered estimate of D to exceed the known value by an amount $\sigma_\eta^2/\Delta t$, where σ_η^2 is the variance of the error. Both temporal averaging and random noise have the largest affect on

the high-frequency part of the spectrum. Averaging removes power at high frequency, whereas random error introduces power across all frequencies, although it is most evident at high frequency. Consequently, the low-frequency part of the spectrum is relatively unaffected by both sources of error. We exploit this result to construct a broadband paleomagnetic power spectrum.

4. A Composite Paleomagnetic Power Spectrum

We use two sources of information to construct the paleomagnetic spectrum. Model PADM2M of Ziegler et al. (2011) gives the axial dipole moment over the past 2 Myr at intervals of 1 kyr, whereas CALS10K2 (Constable et al., 2016) gives the axial dipole moment (and other low-degree components of the magnetic field) over the past 10 kyr at intervals of 50 years. Figure 6 shows the power spectrum for each model, calculated using a multi-taper method (function pmtm in Matlab). We also show two theoretical spectra. One spectrum is predicted using the parameters of a simple stochastic model derived from PADM2M (Buffett et al., 2013). We take $\gamma = 34$ Myr^{-1} and let $D_{eq} = 69 \times 10^{44}$ A^2 m^4 Myr^{-1} (or 0.069×10^{44} A^2 m^4 kyr^{-1}). The second spectrum is obtained by applying a gaussian filter to the stochastic model, using an averaging time of $T = 2.4$ kyr. The sampling used to construct the stochastic model from PADM2M was $\Delta t = 5$ kyr, so the filter required to account for the power spectrum of PADM2M is broadly compatible with the proposed rule of thumb $\Delta t \approx 2T$.

CALS10K2 possesses more power than PADM2M at overlapping frequencies. One interpretation is that temporal averaging has a greater influence on PADM2M, which acts to reduce the power at high frequencies. We might

remedy this problem by seeking an independent estimate for the noise term from CALS10K2. Figure 7 shows the resulting estimates for D as a function of Δt. The noise term initially increases with Δt, implying some temporal averaging or possibly correlated noise in the stochastic model. A simple parametric fit of the form

$$D(\Delta t) = D_{eq}(1 - e^{-\Delta t/T}) \tag{22}$$

gives $D_{eq} = 0.34 \times 10^{44}$ A^2 m^4 kyr^{-1} (340×10^{44} A^2 m^4 Myr^{-1}) for the asymptotic value of the noise term. We fit (22) through the lower limit of the estimates in Fig. 7 to account for the influence of random error (which tends to increase D). A correlation time of $T = 120$ years suggests that the sampling of the stochastic process should be restricted to $\Delta t > 240$ years. (We adopt $\Delta t = 300$ years as a lower limit in our subsequent discussion.) The value of the noise term recovered from CALS10K2 is more than four times larger than the value we recovered from PADM2M, but it can account for the higher power in the CALS10K2 spectrum.

Simply increasing the value of D in the stochastic model predicts more power at low frequencies, which is incompatible with the low-frequency part of the PADM2M spectrum. Since we expect random error and temporal averaging to have less affect at low frequencies, we choose to alter both D and γ to maintain agreement with PADM2M at low frequencies. In effect, we are use the low-frequency spectrum of PADM2M to estimate γ once D is inferred from CALS10K2. The predicted power at low frequency is D/γ^2, so we take $\gamma = 75 \times 10^{22}$ A m^2 Myr^{-1} and $D = 340 \times 10^{44}$ A^2 m^4 Myr^{-1} to retain consistency with the low-frequency power in PADM2M. While the slope of the drift term is more than twice the value recovered from PAD2M

using (4), it is in rough agreement with the value $\gamma = 70 \times 10^{22}$ A m^2 Myr^{-1} estimated for the PISO-1500 model (Channell et al., 2009). (The noise term for PISO-1500 near $x =< x >$ is 540×10^{44} A^2 m^4 Myr^{-1}, which is somewhat higher than the value recovered from CALS10K2. Interestingly, the preferred sampling interval for PISO-1500 is 4 to 5 kyr, which is close to the sampling interval adopted previously for PADM2M and SINT-2000 (Buffett et al., 2013). Thus the time averaging in all three VADM models is roughly the same).

We test the revised values for γ and D by running a series of 100 realizations of the stochastic model. The model parameters are fixed but the initial conditions and details of the each realization differ. The realizations are run for 2 Myr and the value of the dipole moment is recorded every 300 years, corresponding to the sampling interval inferred from CALS10K2. It is possible that the short averaging time (nominally 120 years) corresponds to the lifetime of convective eddies in the core. We could account for this effect in the stochastic model by introducing a correlated noise source (Buffett and Matsui, 2015), but we avoid this complication by choosing Δt to ensure the noise source, $\Gamma(t)$ is uncorrelated. A power spectrum is computed for each realization and the results are superimposed on the power spectra computed from PADM2M and CALS10K2 (see Fig 8a). The cloud of power spectra for the realizations overlap the low-frequency part of the PADM2M power spectrum and most of the power spectrum for CALS10K2 below 1 cycle/kyr. However, a direct comparison of the realizations with the power spectrum for CALS10K2 is not appropriate because the CALS10K2 spectrum is computed from a 10-kyr time series. A better comparison would rely on 10-kyr

realizations (see Fig8b). A series of shorter realizations produces a cloud of power spectra that overlap the computed power spectrum for CALS10K2, suggesting that the revised stochastic model is broadly consistent with the CALS10K2 model.

We also test the stochastic model against historical observations (Jackson et al., 2000). A steady decrease in the dipole field has lowered the dipole moment by $\Delta x = 0.68 \times 10^{22}$ A m^2 over a 150-year interval between 1860 and 2010 (Gillet et al., 2013). Such a change is too large to be caused by the drift term, so it must be associated with the noise term. The root-mean-square (rms) variation in the dipole moment due to the noise term is $< \Delta x^2 >^{1/2} = \sqrt{2D\Delta t}$. Using the revised estimate of D and $\Delta t = 0.15$ kyr, we find $< \Delta x^2 >^{1/2} = 0.32 \times 10^{22}$ A m^2. Thus the historical variation is larger than the expected variation, but it is not implausible. A realization of the noise process is described by (Risken, 1989)

$$\Delta x = \sqrt{2D\Delta t}\, w \tag{23}$$

where w is a random variable drawn from a standard normal distribution (mean of zero and variance of 1). We require $w = 2.13$ to account for the recent variation in the dipole field, which would occur about 1.7% of the time. The actual probability could be somewhat lower if the noise source is correlated at $\Delta t = 0.15$ kyr (a likely case given our estimate of the correlation time from CALS10K2). The preceding estimate would then represent an overestimate of the probability of occurrence. By comparison, the original value of $D = 0.069 \times 10^{44}$ A^2 m^4 kyr^{-1} from PADM2M would require $w = 4.73$ to account for the historical variation. Such an event would occur less than 0.0001% of the time. Such an event is fairly unlikely, so the historical record

lends support to the larger value for the noise term.

Another useful prediction of the stochastic model is the variance of the dipole moment. We obtain an expression for the variance, σ_x^2, by integrating the power spectrum over frequency

$$\sigma_x^2 = \int_{-\infty}^{\infty} S_\epsilon(f)\, df = \frac{D}{\gamma}\,. \tag{24}$$

The revised values for $D = 0.34 \times 10^{44}$ A^2 m^4 kyr^{-1} and $\gamma = 0.075$ kyr^{-1} give $\sigma_x = 2.13 \times 10^{22}$ A m^2. While this value exceeds the estimate $\sigma_x = 1.48 \times 10^{22}$ A m^2 for PADM2M (Ziegler et al., 2011), it is not too far from the estimate $\sigma_x = 1.97 \times 10^{22}$ A m^2 for SINT-2000 (Valet et al., 2005) and somewhat smaller than the estimate $\sigma_x = 2.68 \times 10^{22}$ A m^2 for PISO-1500 (Channell et al., 2009). Thus the predicted variance lies within the range of estimates from recent VADM models.

5. Geomagnetic Polarity Reversals

A more general representation of the drift term is needed to describe geomagnetic polarity reversals. The linear approximation in (6) is useful when x varies about $< x >$, but its utility ceases when x approaches zero during a reversal. The invariance of the magnetic induction equation to a change in the sign of the magnetic field suggests that $v(x)$ is an odd function of x. We expect the drift term to adjust x toward the negative value of the time average once x changes sign. A simple extension of the linear approximation is

$$v(x) = -\frac{\gamma\, x}{< x >}(x - < x >) \quad \text{for } x \geq 0\,, \tag{25}$$

where the expected symmetry is obtained by taking $v(-x) = -v(x)$. The gradient of $v(x)$ at $x =< x >$ is consistent with the linear approximation

in (6), but the value of the drift now vanishes at $x = 0$. It is convenient to represent the drift as the negative gradient of a potential $U(x)$. Integrating (25) for the $U(x)$ gives

$$U(x) = \frac{1}{2}\frac{\gamma x^2}{< x >}\left[\frac{2}{3}x - < x >\right] \quad \text{for } x \geq 0 \tag{26}$$

where the integration constant is chosen to make $U(0) = 0$. A comparison of $U(x)$ with the potential recovered from the PADM2M model of Ziegler et al. (2011) is shown in Fig. 9. The barrier at $x = 0$ is comparable for both potentials, but the amplitudes of $U(x)$ at large $|x|$ differ. This is mainly a consequence of increasing γ in the revised stochastic model. A larger γ produces a narrower potential well and limits the variability of x at a fixed level of noise, consistent with the predicted standard deviation $\sigma_x = \sqrt{D/\gamma}$. We now use the generalization of the drift in (25) to predict the rate of magnetic reversals and the duration of polarity transitions.

5.1. Rates of Reversals

Random fluctuations in x enable the dipole to jump from one potential well to the other, leading to a magnetic reversal. The average frequency of this transition can be predicted using the stochastic model. Kramers (1940) derived an approximation expression for the reversal rate, r, when the barrier $\Delta U = U(0) - U(< x >)$ is large compared with the noise D. Kramers' formula in our notation gives

$$r = \frac{\gamma}{2\pi} e^{-\Delta U/D}\,. \tag{27}$$

Substituting for

$$\Delta U = \frac{1}{6}\gamma < x >^2 \tag{28}$$

from (26) and using the definition of the variance from (24) gives

$$r = \frac{\gamma}{2\pi} e^{-<x>^2/(6\sigma_x^2)} \ . \tag{29}$$

Remarkably, the rate of reversal depends on the time average, $< x >$, the variance, σ_x^2, and the timescale for slow adjustments of the dipole field, γ^{-1}; the slow timescale is thought to reflect the decay time of dipole fluctuations (e.g. Gubbins and Roberts, 1987). Geodynamo simulations suggest that the dipole fluctuations can be represented by the first few decay modes (Buffett et al., 2014). Using $< x >= 5.3 \times 10^{22}$ A m^2, $\sigma_x = 2.13 \times 10^{22}$ A m^2 and $\gamma = 75$ Myr^{-1} gives $r = 4.2$ reversals per Myr, which is comparable to the observed rate over the past 30 Myr (Lowrie and Kent, 2004). By comparison, a 60-Myr realization of the stochastic process yields 3.9 reversals per Myr when the realization is filtered to a resolution of 30 kyr, comparable to the resolution of marine magnetic anomalies (Gee and Kent, 2015). The need to filter the realization is connected to the complexity of polarity transitions when the noise term is large. We explore this question in the next section.

5.2. Duration of Polarity Transitions

The duration of polarity transitions depends on how the transitions are defined. A definition based on magnetic intensity might depend on the time required for the dipole to recover to the long-term average after a change in sign (i.e. a recovery time). This particular definition is useful for our purposes because it can be computed from the stochastic model. We expect the drift term to be small near $x \approx 0$, so the evolution of the dipole during the transition is dominated by the noise term. A useful approximation for the time required for the field to rise above a particular threshold, x_t, is

(Buffett, 2015)

$$\tau = \frac{4x_t^2}{D(0)\pi^2} \tag{30}$$

where $D(0)$ refers to the value of the noise term at $x = 0$. The general form of (30) is characteristic of a diffusive process, which includes no contribution from the drift term. A more exact treatment of the problem accounts for the drift term as x rises toward the threshold x_t. Figure 10 shows a comparison of the approximation in (30) with the value computed from a numerical solution of the Fokker-Planck equation (e.g. Risken, 1989). Including the drift term shortens the recovery, but the difference is relatively small when we adopt the revised value for D. This implies that the recovery of the magnetic field following a reversal is driven mainly by noise (e.g. random turbulent fluctations in the field generation).

We can compute a recovery time from the PADM2M model by interpolating the time when x rises above the time average after a reversal. Each reversal gives a different value for τ, but the average and its standard deviation are shown in Fig. 10. The agreement with theory is surprisingly good. We also show the time required for the field to drop from the time-averaged value into a reversal (i.e. a decline time). The mean decline time from PADM2M is 41 kyr, whereas the mean recovery time is 27 kyr. This asymmetry is consistent with previous observations (Valet and Meynadier, 1993). (The decline time was incorrectly reported as the recovery time in Buffett (2015), although the main point in that study was that these short durations require a noise term in excess of 300×10^{44} A^2 m^4).

The difference between the recovery and decline times can be attributed to the role of the drift term. The recovery time is shorter than the ap-

proximation in (30) because the drift term drives the dipole moment toward the time average, increasing the rate of adjustment after a reversal. Conversely, the dipole must work against the drift term during the decline phase. The approximation in (30) lies roughly midway between the estimates from PADM2M, which suggests that the drift lengthens and shortens the adjustment by comparable amounts, relative to a purely diffusive process with no drift term.

It is reasonable to question whether the PADM2M model can adequately resolve the recovery time when the short-period behavior is not sufficient to compute D. A transition that lasts $\tau \approx 30$ kyr would correspond to a frequency of $f = 1/2\tau$, assuming the transition represents half a cycle. A nominal frequency of 0.017 cycles kyr^{-1} lies in the part of the spectrum where PADM2M and the stochastic model are broadly consistent (see Fig. 8). Consequently, there is internal consistency in our argument that the stochastic model is in agreement with both the transition duration and low-frequency power spectrum from PADM2M. It is encouraging that the same stochastic model gives a reasonable estimate for the reversal rate, particularly when no information about the reversal rate is used in the construction of the stochastic model.

The dominance of the noise term during a polarity transition has interesting consequences for the complexity of reversals. A process that is driven solely by the noise term is analogous to a random walk. The probability of stepping back and forth across $x = 0$ increases with the number of steps n. Dasgupta and Rubin (1998) show that the expected number of zero-crossings is proportional to $\sqrt{n}$. As we decrease the step size in a numerical realiza-

tion, we take a large number of steps through the transition and produce a large number of zero-crossings during a single transition. In practice the time step is limited by the correlation time of the noise source. Independent realizations of the noise process require the time step to exceed the correlation time of the noise, so the number of steps through a transition cannot be arbitrarily large. Still, several zero crossings are likely.

Numerical realizations with $D(0) = 0.3 \times 10^{44}$ A^2 m^4 kyr^{-1} (close to the value proposed here) produced multiple zero-crossings in about 50% of the polarity transitions when $\Delta t = 1$ kyr (Buffett, 2015). The average number of zero crossings is 2.8, but this number would go up if $\Delta t = 0.3$ kyr is a more reasonable estimate for the time step. We could expect $3\times$ more time steps through a transition and roughly $\sqrt{3}\times$ more zero crossings (on average), corresponding to a total of 5 changes in sign during a transition. To make meaningful comparisons with geological observations we would want to remove these short-period polarity changes by filtering the numerical realization to the resolution of the observations. In the previous section we used $T = 30$ kyr to compare the reversal rate with estimates from marine magnetic anomalies.

6. Conclusions

Stochastic models have been successfully tested using geodynamo simultions, but their use with paleomagnetic observations requires departures from the standard approach. Two main difficulties are identified. The first is due to random error in the estimates of the dipole moment, which cause the noise term to be over-estimated. The significance of this problem depends

on the sampling interval, Δt, and the largest affects occur at short Δt. A second difficulty arises from temporal averaging of dipole fluctuations, either due to errors in dating or gradual acquisition of magnetization in sediment. In either case, temporal averaging reduces the noise term at short Δt, although estimates for D often converge to a constant value as Δt increases. Unfortunately, the noise term does not necessarily converge to the correct value.

An important feature of both random error and temporal averaging is that the largest influence is predicted at high frequency. Because the low-frequency behavior is less affected, we can use the low-frequency part of the observed power spectrum as a constraint on the stochastic model. We illustrate the approach using the PADM2M model of Ziegler et al. (2011) and the CALS10K2 model of Constable et al. (2016). An estimate of the noise term is recovered from the high-resolution CALS10K2 model, while the slope of the drift term, γ, is estimated from the low-frequency part of the spectrum for PADM2M. Realizations of the stochastic model yield a composite power spectrum that agrees reasonably well with both PADM2M and CALS10K2.

A simple generalization of the stochastic model is needed to allow large deviations from the time-averaged moment. This modification enables predictions for the mean rate of reversal. A reversal in the stochastic model occurs when a realization jumps between the minima in a double-well potential. Application of Kramers' formula (Kramers, 1940) gives a surprisingly simple expression for the reversal rate. We find that the reversal rate can be defined in terms of the time-averaged dipole moment, the variance of the dipole moment and a slow timescale that characterizes the adjustment of

the dipole toward the time-averaged value. Using values from the stochastic model gives a mean rate of 4.2 Myr^{-1}, which is good agreement with observations (Lowrie and Kent, 2004). Comparable rates are obtained from realizations of the stochastic process, provided we filter the realization to the same resolution as the observations. The need for temporal filtering arises from the importance of noise in driving polarity transitions. Multiple polarity changes can occur within a single transition field, so a quantitative comparison with observations depends on the temporal resolution of those observations.

Acknowledgment

This work is supported by the National Science Foundation (EAR-1644644) and by a Summer Undergraduate Research Fellowship (SURF) from Caltech.

Brendel, K., Kuipers, J., Barkema, G.T., Hoyng, P., 2007. An analysis of the fluctuations of the geomagnetic dipole, *Phys. Earth Planet. Inter.*, *162*, 249-255.

Bouligand, C., Gillet, N., Jault, D., Schaeffer, N., Fournier, A. and Aubert, J., 2016. Frequency spectrum of the geomagnetic field harmonic coefficients from dynamo simulations, *Geophys. J. Int.*, *207*, 1142-1157.

Bracewell, R., 1999. *The Fourier Transform and its Applications*, 3rd ed., McGraw-Hill, New York.

Buffett, B.A., Ziegler, L. and Constable, C.G., 2013. A stochastic model for palaeomagnetic field variations, *Geophys. J. Int.*, *195*, 86-97.

493 Buffett, B.A., King, E.M. and Matsui, H., 2014. A physical interpretation of
494 stochastic models for fluctuations in the Earth's dipole, *Geophys. J. Int.*,
495 *199*, 597-608.

496 Buffett, B. and Matsui, H., 2015. A power spectrum for the geomagnetic
497 dipole moment, *Earth Planet. Sci. Lett.*, *411*, 20-26.

498 Buffett, B., 2015. Dipole fluctuations and the duration of geomagnetic po-
499 larity transitions, *Geophys. Res. Lett.*, *42*, 7444-7451.

500 Channell, J.E.T., Xuan, C., and Hodell, D.A., 2009. Stacking paleointensity
501 and oxygen isotope data for the last 1.5 Myr (PISO-1500), *Earth Planet.*
502 *Sci. Lett.*, *283*, 14-23.

503 Constable, C. and Johnson, C., 2005. A paleomagnetic power spectrum,
504 *Phys. Earth Planet. Inter.*, *153*, 61-73.

505 Constable, C., Korte, M. and Panovska, S., 2016. Persistent high paleosecular
506 variation activity in southern hemisphere for at least 10,000 years, *Earth*
507 *Planet. Sci. Lett.*, *453*, 78-86.

508 Dasgupta, A. and Rubin, H., 1998. Zero crossings of a gaussian process ob-
509 served at discrete random times and some peculiar connections to the
510 simple random walk, *Technical Report 97-23*, Department of Statistics,
511 Purdue University, West Lafayette, IN.

512 Friedrich, R., Peinke, J., Sahimi, M., and Reza Rahimi Tabar, M., 2011.
513 Approaching complexity by stochastic methods: From biological system
514 to turbulence, *Phys. Rep.*, *506*, 87-162.

Gee, J.S. and Kent, D.V., 2015. Sources of oceanic magnetic anomalies and the geomagnetic polarity timescale, *Treatise on Geophysics*, 2nd Ed., *Vol. 5*, 419-460.

Gillet, N., Jault, D., Finlay, C. and Olsen, N., 2013. Stochastic model of the Earth's magnetic field: Inversion for covariances over the observatory era, *Geochem. Geophys. Geosys.*, *14*, 766-786.

Gubbins, D. and Roberts, P.H., 1987. Magnetohydrodynamics of the Earth's core, in *Geomagnetism*, vol. 2, ed. Jacobs, J.A., Academic Press.

Hoze, N. and Holeman, D., 2015. Recovering a stochastic process from super-resolution noisy ensembles of single particle trajectories, *Phys. Rev. E.*, *92*, 052109.

Jackson, A., Jonker, A.R.T., and Walker, M.R., 2000. Four centuries of geomagnetic secular variation from historical records, *Phil. Trans. R. Soc. Lond. A*, *358*, 957-990.

Kramers, H.A., 1940. Brownian motion in a field of force and the diffusion model of chemical reactions, *Physica*, *7*, 284-304.

Kuipers, J., Hoyng, P., Wicht, and Barkema, G.T., 2009. Analysis of the variability of the axial dipole moment of a numerical geodynamo model, *Phys. Earth Planet. Inter.*, *173*, 228-232.

Korte, M. and Constable, C.G., 2011. Improving geomagnetic field reconstructions for 0-3 ka, *Phys. Earth Planet. Inter.*, *188*, 247-259.

Leonard, A., 1974. Energy cascade in large-eddy simulations of turbulent flows, *Adv. Geophys.*,*18*, 237-248.

Lowrie, W. and Kent, D.V., 2004. Geomagnetic polarity timescale and reversal frequency regime, in Channell, J.E.T, Kent, D.V., Lowrie, W. and Meert, J., (eds.) *AGU Geophysical Monograph*, *145*, Timescales of the Paleomagnetic Field, 117-129, Washington DC, American Geophysical Union.

Matsui, H., King, E. and Buffett, B., 2014. Multi-scale convection in a geodynamo simulation with uniform heat flux along the outer boundary, *Geochem. Geophys. Geosys.*, *15*, doi: 10.1029/2014GC005432.

Meduri, D.G. and Wicht, J., 2016. A simple stochastic model for dipole moment fluctuations in numerical dynamo simulations, *Front. Earth Sci.*, *4*, doi: 10.3389/feart.2016.00038.

Langevin, P., 1908. Sur la théorie due mouvement brownien, *C. R. Acad. Sci.*, *146*, 530-533.

Olson, P., Christensen, U.R., and Driscoll, P.E., 2012. From superchrons to secular variations: A broadband dynamo frequency spectrum for the geomagnetic dipole, *Earth Planet. Sci. Lett.*, *319*, 75-82.

Percival, D.B. and Walden, A.T., 1993. *Spectral analysis for physical applications: multi taper and conventional univariate techniques*, Cambridge University Press, Cambridge.

Risken, H., 1989. *The Fokker-Planck Equation*, 2nd Ed., Springer-Verlag.

557 Roberts, A.P. and Winkholfer, M., 2004. Why are geomagnetic excursions
558 not always recorded in sediments? Constraints from post-depositional re-
559 manent magnetization lock-in modeling, *Earth Planet. Sci. Lett.*, *227*, 345-
560 359.

561 Sakuraba, A. and Hamano, Y., 2007. Turbulent structure in Earth's fluid
562 core inferred from time series of geomagnetic dipole moment, *Geophys.*
563 *Res. Lett.*, *34*, L15308, doi: 10.1029/2007GL029898.

564 Valet, J.-P., Meynadier, L., 1993. Geomagnetic field intensity and reversals
565 during the past four million years, *Nature*, *366* 234-238.

566 Valet, J.-P., 2003. Time variations in geomagnetic intensity, *Rev. Geophys.*,
567 *41*, 1004, doi: 10.1029/2001RG000104.

568 Valet, J.-P., Meynadier, L., Guyodo, Y., 2005. Geomagnetic field strength
569 and reversal rate over the past 2 million years, *Nature*, *435*, 802-805.

570 Van Kampen, N.G., *Stochastic Methods in Physics and Chemistry*, North-
571 Holland, Amsterdam.

572 Ziegler, L.B., Constable, C.G., Johnson, C.L., Tauxe, L., PADM2M: a penal-
573 ized maximum likelihood model of the 0-2 Ma paleomagnetic axial dipole
574 moment, *Geophys. J. Int.*, *184*, 1069-1089.

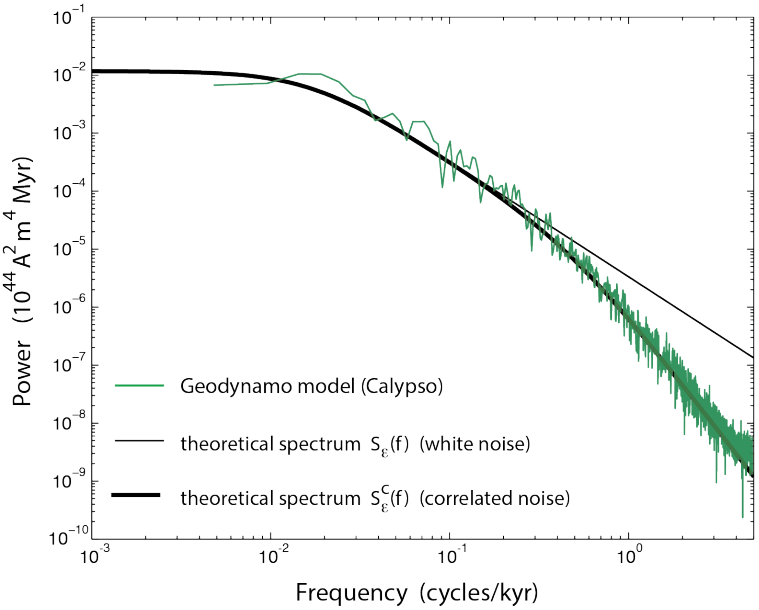

Figure 1: A power spectrum of dipole fluctuations from a numerical geodynamo simulation (Matsui et al., 2014), compared to predictions from two stochastic models. One stochastic model assumes a white noise source and the other assumes correlated noise. Both models are capable of predicting the low-frequency fluctuations even though the drift and diffusion terms are constructed from short-period information.

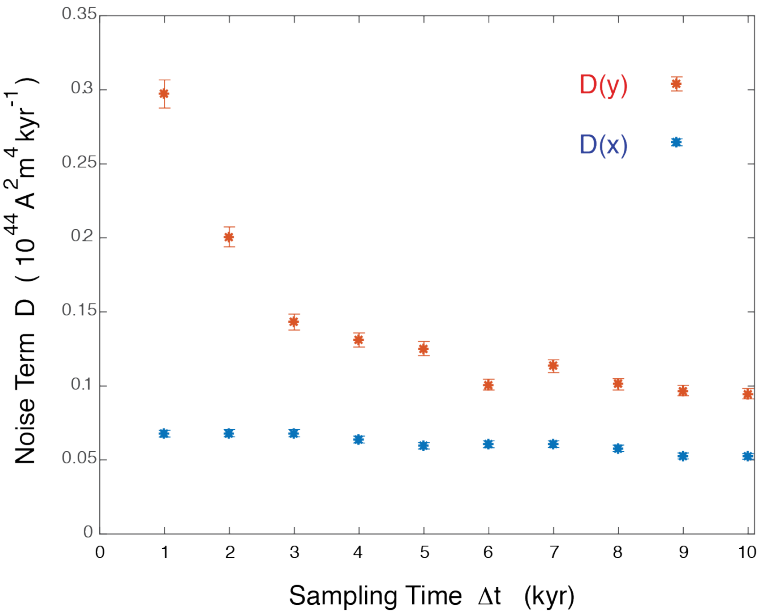

Figure 2: Estimates for the noise term, D, computed from exact $x(t)$ and noisy $y(t)$ time series. Addition of random error to $y(t)$ causes $D(y)$ to depart from the known value $D = 0.069 \times 10^{44}$ A^2 m^4 kyr^{-1}. Calculations using $x(t)$ reproduce the known value to within the uncertainties at $\Delta t = 1$ kyr. Discrepancies in $D(x)$ increase with Δt due to unmodelled contributions from higher-order powers in Δt.

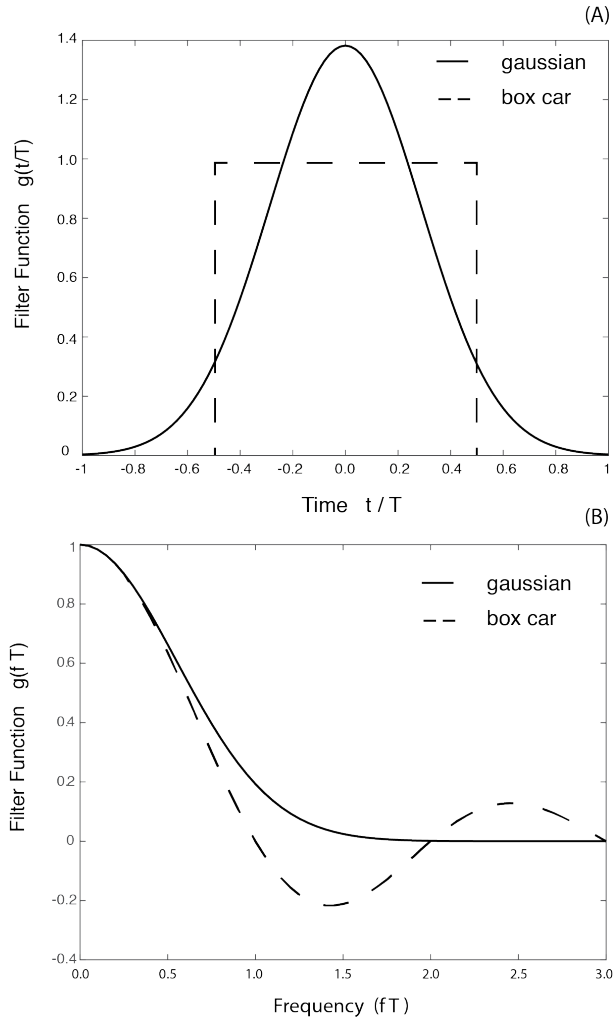

Figure 3: (A) Two commonly used filters are the gaussian, $g(t) = (6/\pi T^2)^{1/2} \exp(-6t^2/T^2)$, and the box car, $g(t) = 1/T$ for $|t| < T/2$, where T is the averaging time. (B) Fourier transforms are given by $g(f) = \exp(-4\pi^2 f^2 T^2/24)$ and $g(f) = \sin(\pi f T)/\pi f T$, respectively.

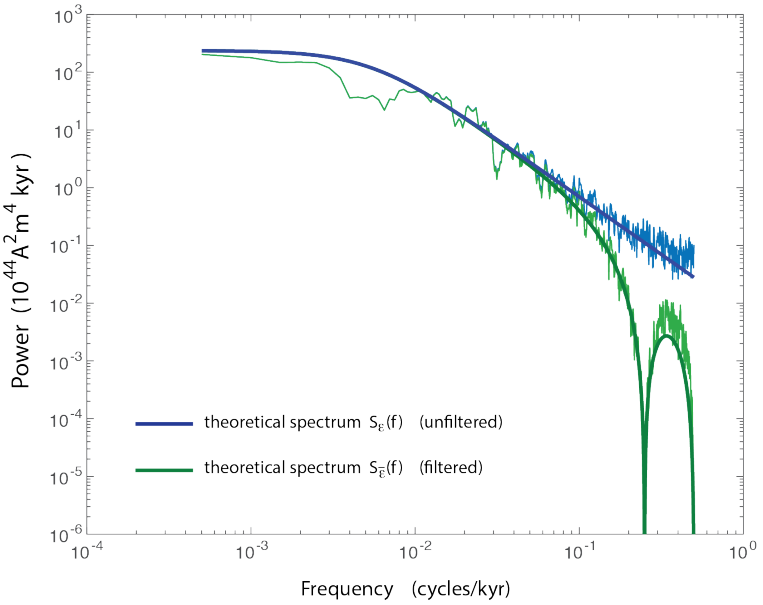

Figure 4: Power spectra of $x(t)$ (blue) and $\bar{x}(t)$ (green) compared with theoretical spectra $S_\epsilon(f)$ and $S_{\bar{\epsilon}}(f)$ (see text). Undulations in the filtered spectrum arise from the box-car filter, which is oscillatory in the frequency domain.

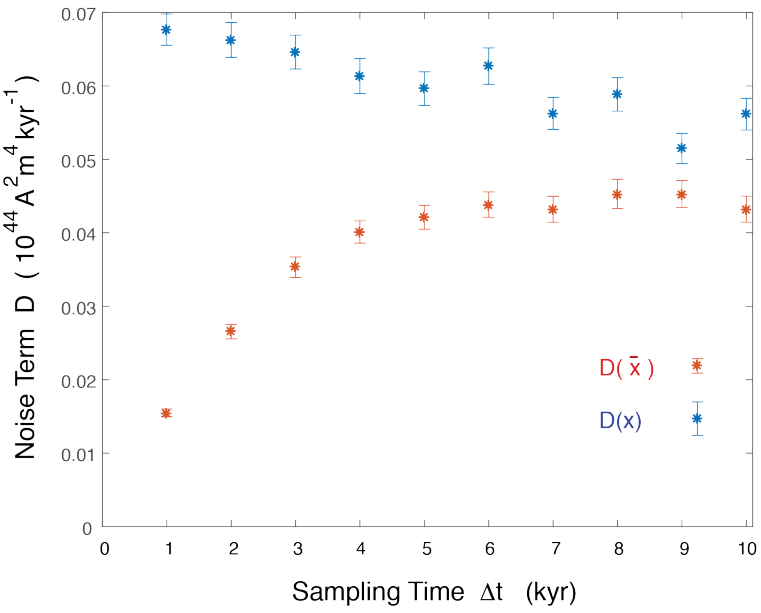

Figure 5: Estimates for the noise term, D, computed from exact $x(t)$ and filtered $\bar{x}(t)$ time series. Temporal averaging substantially reduces the noise term when Δt is less than the averaging time $T = 3$ kyr. Estimates for $D(\bar{x})$ approach a constant value once $\Delta t > 2T$.

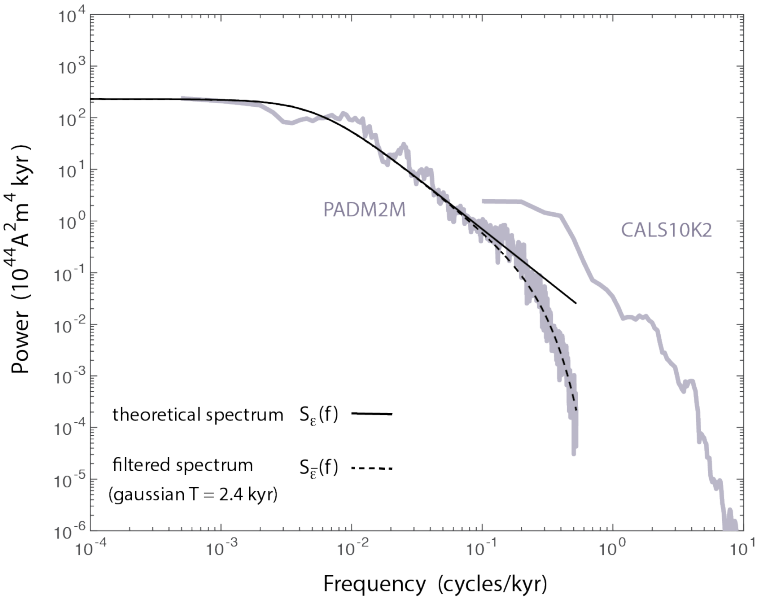

Figure 6: Power spectra computed from PADM2M and CALS10K2 using a multi-taper method. Theoretical spectra $S_\epsilon(f)$ and $S_{\bar{\epsilon}}(f)$ are based on the stochastic model derived from PADM2M and a filtered version of the stochastic model. We apply a gaussian filter with an averaging time of $T = 2.4$ kyr to account for the abrupt decrease in power of PADM2M at high frequency.

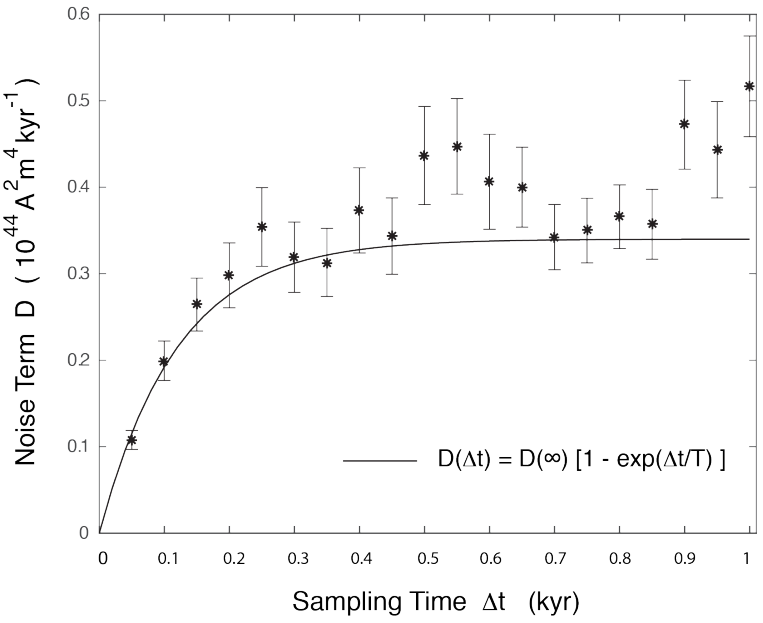

Figure 7: Estimates for the noise term, D, recovered from CALS10K2 as a function of sampling time Δt. A simple parametric fit to $D(\Delta t)$ in (22) gives $D(\infty) = 0.34 \times 10^{44}$ A^2 m^4 kyr^{-1}. The effective correlation time of the noise source is $T = 120$ years.

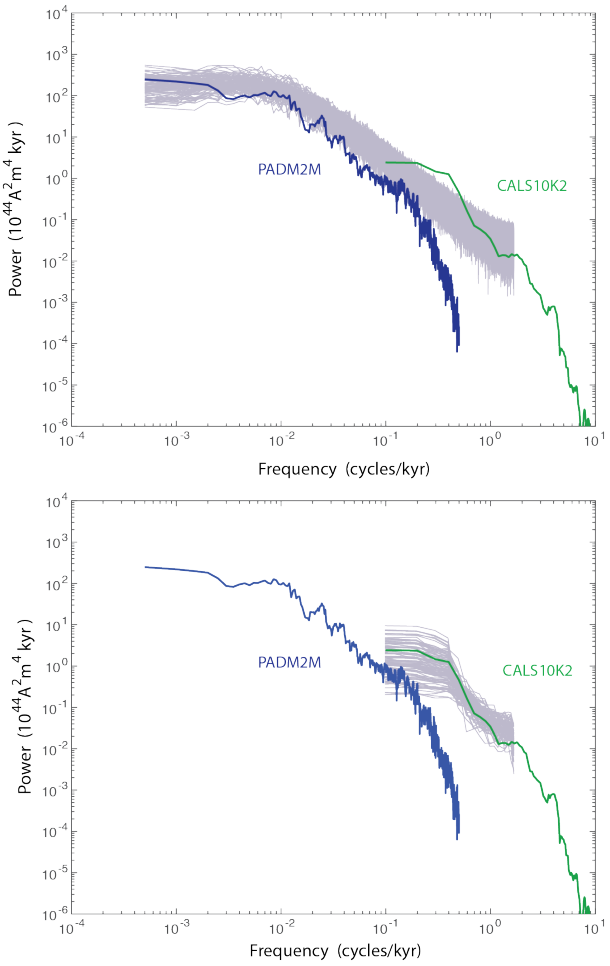

Figure 8: (A) Power spectra from 100 realizations of the stochastic model (in gray) compared with the power spectra computed from PADM2M (blue) and CALS10K2 (green). The ensemble of realizations is compatible with PADM2M at low frequencies and much of the spectrum for CALS10K2 below 1 cycle/kyr. (B) Power spectra of 100 shorter (10-kyr) realizations of the stochastic model.

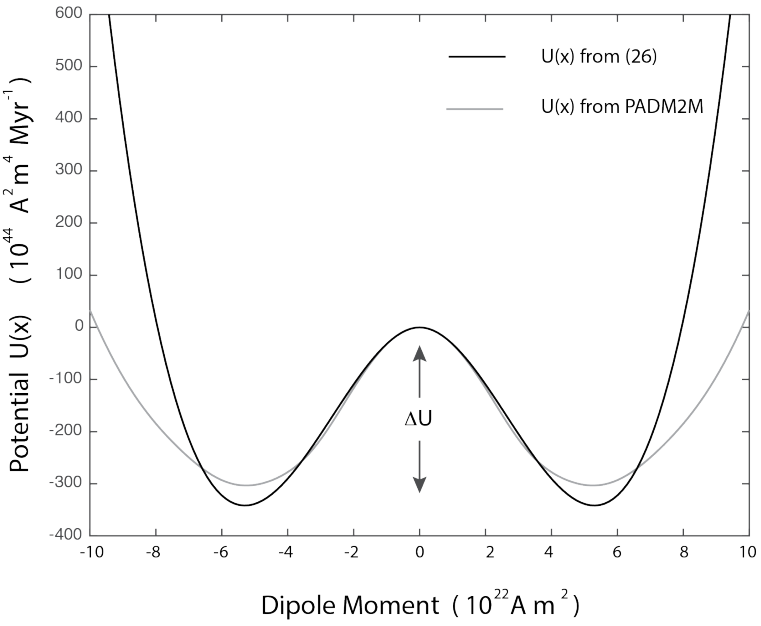

Figure 9: Potential $U(x)$ computed from (26) compared with a potential recovered from PADM2M. Both potentials have comparable barriers, ΔU, but different amplitudes at large $|x|$. The width of the potential well is defined by the second derivative $U''(x) = -\gamma$ at $x = \pm < x >$. We use $\gamma = 73$ Myr^{-1} for the potential in (26), but obtained $\gamma = 34$ Myr^{-1} from PADM2M.

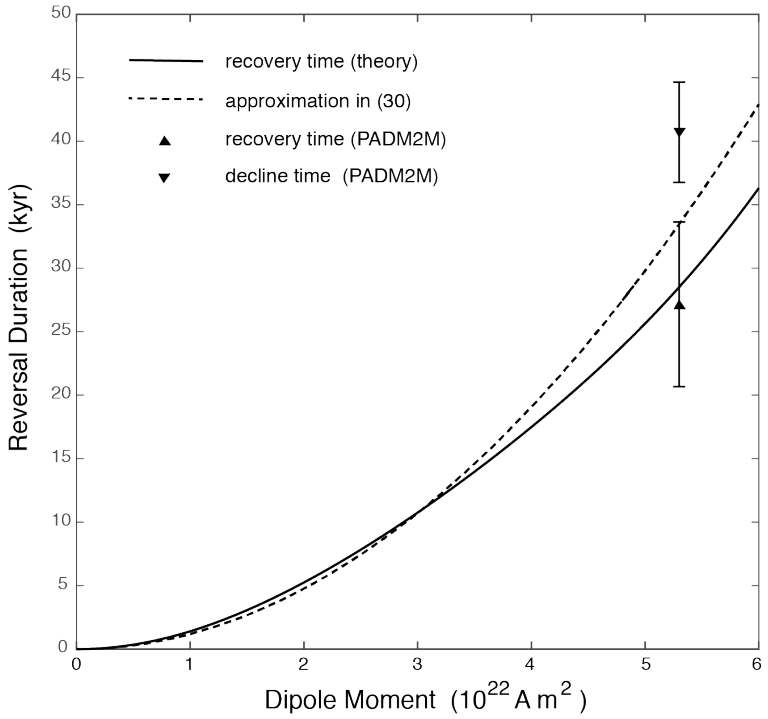

Figure 10: Mean recovery time for the dipole moment following a reversal. A numerical solution of the Fokker-Planck equation (theory) is compared with the approximation in (30), where the drift term is assumed to vanish. Discrete estimates from PADM2M are shown for the recovery and decline times. The recovery time agrees well with theory, whereas the decline time exceeds the recovery time, probably due to contributions from the drift term. The approximation in (30), which includes no contribution from the drift term, lies roughly midway between the recovery and decline times from PADM2M.